PNAS RESEARCH ARTICLE | MEDICAL SCIENCES

Senolytic treatment induces oligodendrocyte dysfunction and demyelination in the corpus callosum

Evan R. Lombardo[a,1], Robert S. Pijewski[a,1,2], Jake T. Lustig[a], Zaenab Dhari[a,b,c], Anirudhya Lahiri[a], Lucille E. Papile[a], Erica R. Lavoie[a], Vanessa M. Scanlon[d], Jenna M. Bartley[e,f], and Stephen J. Crocker[a,f,3]

Affiliations are included on p. 9.

Edited by Lawrence Steinman, Stanford University Arnold and Mabel Beckman Center for Molecular and Genetic Medicine, Stanford, CA; received September 5, 2025; accepted January 22, 2026

Aging is a primary risk factor for disease progression in multiple sclerosis (MS). Because of this, treatments that can reduce the consequences of molecular aging, like senescence, have been proposed as a strategy to address disease progression. However, the effects of senolytics, a class of drugs which selectively ablate senescent cells, on the central nervous system are largely unknown. Here, we examined the effects of senolytic treatment on myelination and oligodendrocyte function in vivo using C57BL6/J mice and in vitro using primary rat oligodendrocyte cultures. Initial data showed that naïve young (3 to 4 mo) and aged (22 mo) C57BL6/J mice treated with dasatinib and quercetin (D+Q) developed significant demyelination compared to vehicle-treated controls, though no cell death was observed in the brain. In vitro, oligodendrocyte progenitor cells treated with D+Q in differentiation media exhibited significantly reduced myelin basic protein protein and morphological complexity, also without inducing cell death. Bulk RNA sequencing and ingenuity pathway analysis of D+Q treated oligodendrocytes identified differentially expressed genes associated with endoplasmic reticulum stress. These data suggest that D+Q evokes the unfolded protein response in oligodendrocytes, causing oligodendrocyte dysfunction and myelination failure. Due to the resemblance between oligodendrocytes treated with D+Q and those found in MS lesions, D+Q treatment offers a potential method to model an aspect of oligodendrocyte dysfunction relevant to MS. Therefore, understanding the mechanism by which D+Q perturb oligodendrocyte function may provide insight into some of the pathological features contributing to disease progression in MS.

myelin | oligodedrocyte | aging | demyelination | senescence

Significance

The pharmacological combination of dasatinib and quercetin (D+Q), widely reported as a means of eliminating senescent cells from aged tissues to treat diseases (a.k.a. "senolytics"), and currently being tested in multiple clinical trials, when administered to healthy mice results in profound white matter injury in the central nervous system. This report provides evidence that this senolytic combination not only causes neuropathology but also provides data which support induction of the unfolded protein response as a plausible mechanism through which these senolytics affect oligodendrocytes. We propose that these data highlight a less understood means of demyelination not mediated by oligodendrocyte death with potential positive implications for understanding disease, while also warranting caution for its widespread use clinically.

Aging is a primary risk factor for disease progression in multiple sclerosis (MS) (1–3), an autoimmune disorder characterized by central nervous system (CNS) demyelination that affects 2.8 million people worldwide; older patients have an increased chance of developing progressive MS (PMS), a form of the disease characterized by continuous disease progression and disability accumulation (4). Older patients also display increasing disability accumulation and decreasing responsiveness to disease modifying therapies (DMTs) compared to younger patients (5, 6). Moreover, studies have indicated that patients with MS exhibit accelerated cellular aging compared to age-matched controls (3, 7).

The molecular factors regulating the cellular aging process in disease offer promising therapeutic avenues to improve disease outcomes and ameliorate disability. Cells become senescent after they have reached the Hayflick limit for the maximum number of cell divisions one cell can undergo and no longer divide (8, 9). Senescent cells can be identified by molecular markers like cyclin-dependent kinase inhibitor 1A (CDKN1a), high mobility group box 1 (HMGB1), and Senescence-associated beta-galactosidase (SA-beta-gal). Senescent cells displaying these markers have been shown to be upregulated in demyelinated lesions in the brains of individuals with MS and in neural progenitor cells derived from individuals with MS (7). Furthermore, these senescent cells and senescent factors, like HMGB1, have been shown to directly inhibit oligodendrocyte differentiation and impair remyelination in the brain (7, 10).

Therefore, senolytics, a class of drugs identified to selectively eliminate senescent cells, may provide a means to alter the impact of cellular senescence in the brain (11–18). Dasatinib and quercetin (D+Q) are two drugs that have been reported to deplete senescent cells (12, 16, 18). While dasatinib, a tyrosine kinase inhibitor and BCR-ABL blocker, was initially developed to treat chronic myeloid leukemia (CML), recent studies indicate that it eliminates senescent cells by inhibiting SRC kinase function and preventing AKT phosphorylation (19–23). Quercetin, on the other hand, is a natural flavonoid found in a variety of fruits and vegetables that is reported to have antioxidant and anti-inflammatory

The authors declare no competing interest.

This article is a PNAS Direct Submission.

[1]E.R. Lombardo and R.S.P. contributed equally to this work.

[2]Present address: School of Nursing and Health Science, Anna Maria College, Worcester, MA 01612.

[3]To whom correspondence may be addressed. Email: crocker@uchc.edu.

This article contains supporting information online at https://www.pnas.org/lookup/suppl/doi:10.1073/pnas.2524897123/-/DCSupplemental.

Published March 17, 2026.

properties (24–26). Like dasatinib, quercetin was repurposed as a senolytic after studies showed that it could specifically kill senescent cells (27). D+Q are often used together as it has been reported that the combination of drugs showed increased senolytic potency and targeted a broader range of senescent cell types (15).

Although senolytics have been tested in a variety of disease contexts, little work has been done investigating the effects of senolytics in neurological diseases (28–30). Thus, if senolytics are to be of value for the potential future treatment of MS and other neurological diseases in which senescence has been implicated, more research should be conducted to elucidate the effects of senolytics on the brain in healthy and diseased contexts. Here, we evaluated the impact of D+Q on myelination and oligodendrocyte function in the brain through the treatment of aged and young naive mice, and primary oligodendrocyte cultures.

Results

Effect of Dasatinib and Quercetin (D+Q) on Naïve C57Bl6/J Mice. To determine whether D+Q treatment had any effects on myelination in the brain, we treated a cohort of aged (22 mo) C57Bl6/J mice with senolytics, dasatinib and quercetin (5 mg/kg and 50 mg/kg, respectively), through oral gavage (Fig. 1*A*). This treatment paradigm provides intermittent administration of D+Q which increased posttreatment survival rates of aged mice, as developed by others (31, 32). The brains were fixed and dissected, and the rostral corpus callosum (CC) of each was prepared for transmission electron microscopy (TEM) (Fig. 1*A*). The extent of compact myelination was calculated by g-ratio of myelinated axons in all samples from all subjects (Fig. 1 *D* and *E*). Ratios were then calculated and compared to vehicle-treated, age-matched controls (n > 2,000 axons/group, three mice per group). If D+Q reduces myelination in the brain, D+Q-treated mice would display elevated G-ratios compared to vehicle controls. Significant demyelination was observed in D+Q treated mice when compared to age-matched controls (Fig. 1*C*), an effect that was substantiated quantitatively by an elevated average G-ratio in the brains of D+Q-treated mice compared to vehicle controls (Fig. 1*E*). To determine whether the effect of D+Q was related to age, we treated a cohort of young mice (aged 3 to 4 mo) using the same treatment protocol and analyzed the CC by TEM to determine the degree of compact myelination. This analysis (n

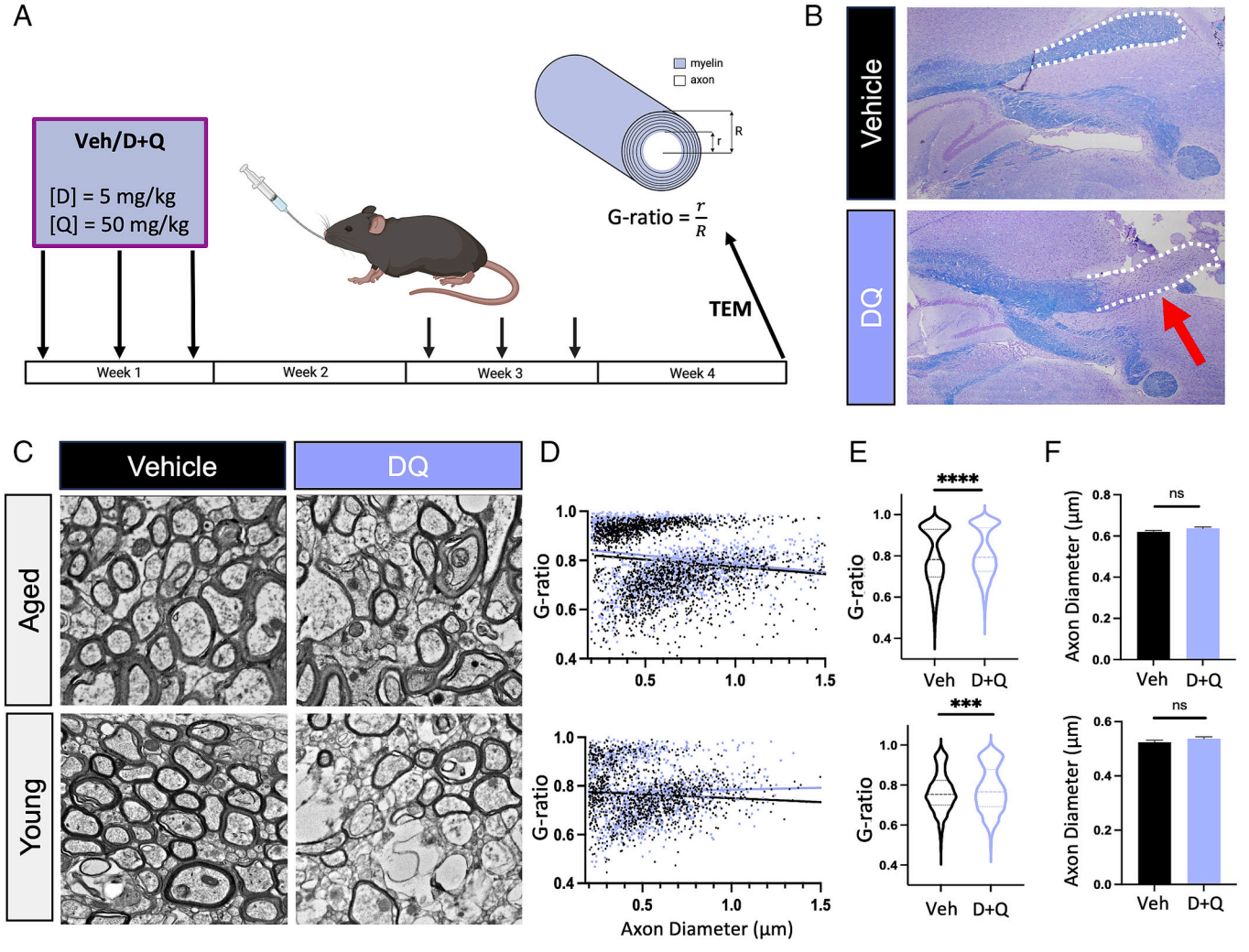

Fig. 1. Senolytic treatment evokes demyelination in aged and young healthy mice. (*A*) Schematic depicting the experimental design. Young (3 mo) and aged (22 mo) mice were administered either dasatinib and quercetin (D+Q) or vehicle via oral gavage three times biweekly (31, 32), after which brain tissues were collected and their rostral corpus callosa prepared for transmission electron microscopy (TEM). (*B*) Luxol fast blue (LFB) staining of the rostrum in brain sections from aged C57Bl6/J mice treated with vehicle or D+Q. (*C*) TEM images from young and aged mice treated with either D+Q or vehicle. (*D–F*) Analysis of G-ratios and axon diameters calculated from aged (*Top*) and young (*Bottom*) D+Q-treated corpus callosum cross-sectional TEM images and compared to vehicle-treated controls. Statistical significance was analyzed utilizing the nonparametric Kolmogorov–Smirnov test. N = 2,000 axons/aged group and n = 1,500 axons/young group ****$P < 0.0001$ ***$P = 0.0001$.

= 1,500 axons/group, three mice per group) also found that D+Q treatment resulted in a significant reduction in compact myelination of axons (Fig. 1*D*). To eliminate a confounding effect resulting from significant differences in axon diameter, the average diameter of axons analyzed were quantified and compared among age-matched treatment groups (Fig. 1*F*). It was noted that there was no significant difference in axon diameters between mice of D+Q treatment or control aged or young groups (Fig. 1*F*). Hence, D+Q induced significant demyelination of the brain of aged or young mice. Interestingly, the negative slope of the trend lines in Fig. 1*D* suggest that D+Q and vehicle treatment affect smaller axons to a greater extent than larger axons in aged mice. However, potential explanations for an axon diameter-dependent effect of D+Q treatment on myelination are unknown and fall outside the scope of the current study.

As TEM can be used to visualize compact but not uncompacted myelin, it is difficult to discern from the images and G-ratio analysis alone whether D+Q treatment induces myelin loss or loss of compact myelination. To distinguish between the two possibilities, we stained brain sections from D+Q and vehicle-treated aged mice with luxol fast blue (LFB), a histological stain used to visualize white matter, and analyzed the corpus callosum, a major white matter tract in the brain. We found that D+Q-treated mice developed significant demyelination in the most anterior, rostral corpus callosum when compared to vehicle-treated controls, but not the body or splenium of the CC (Fig. 1*B*). This validates the hypothesis that D+Q treatment induces myelin loss, albeit in a regionally specific manner. The reasons for regional differences in susceptibility to demyelination are currently unknown and require further investigation.

Senolytic Treatment Blocks Oligodendrocyte Differentiation But Does Not Cause Oligodendrocyte Cell Death. Since oligodendrocytes are the cells responsible for myelinating CNS axons, we hypothesized that D+Q induced demyelination by causing cell death of oligodendrocytes. To test this, we evaluated apoptosis in primary rat oligodendrocyte cultures treated with vehicle, dasatinib, quercetin, or D+Q through a TUNEL assay (Fig. 2*A*). Interestingly, we found no significant difference in cell death between groups (Fig. 2*B*). To further assess the effects of D+Q treatment on oligodendrocyte viability, lactate dehydrogenase (LDH) assays were performed on the media of D+Q- or vehicle-treated oligodendrocytes in vitro (Fig. 2*C*). Similarly, there were no significant differences in LDH levels detected in the media from treated oligodendrocytes compared to controls (Fig. 2*C*), suggesting that oligodendrocyte viability was unaffected following treatment with D+Q. To corroborate these findings in vivo, we performed a TUNEL assay on brain sections from aged mice (22 mo) treated with D+Q or vehicle and found no significant difference (Fig. 2*D*). Furthermore, we performed immunohistochemistry on brain sections from D+Q-treated and vehicle-treated mice, staining against olig2, an oligodendrocyte marker, and cleaved-caspase 3 (CC3), an executioner protein involved in apoptosis, and took images of the CC. We report no significant difference in the number of olig2+ cells or CC3+ olig2+ cells (Fig. 2*D*) within the CC between treatment groups, suggesting that oligodendrocytes within the white matter of the brain remained stable and did not undergo apoptosis as a result of D+Q treatment. Together, these data strongly imply that D+Q does not induce oligodendrocyte death in vivo or in vitro.

To understand the effects of D+Q on the differentiation and maturation of oligodendrocytes, OPCs were treated with D+Q or vehicle in differentiation media (Fig. 2*A*). After 3 d, the proportion of MBP+ cells was significantly reduced in oligodendrocyte cultures treated with D+Q compared to vehicle-treated OPCs, though the number of cells did not change (Fig. 2*F*). These results indicate that D+Q directly inhibited the differentiation of oligodendrocytes *in vitro.* In contrast, mature oligodendrocytes treated with D+Q exhibited no significant difference in the proportion of MBP+ cells compared to controls (Fig. 2*E*). However, we observed a significant decrease in cellular complexity of mature oligodendrocytes treated with D+Q compared to controls (Fig. 2*E*), indicating that D+Q may also hinder process extension of oligodendrocytes. These data suggest that D+Q impairs myelination capacity as it directly prevented OPC differentiation and reduced the average complexity of oligodendrocytes in vitro.

Senolytic Treatment of Mature Oligodendrocytes Evokes Active Process Retraction. To further assess the effects of D+Q on the morphological characteristics of oligodendrocytes, mature oligodendrocytes were treated with dasatinib, quercetin, D+Q, or vehicle and monitored over 24 h using an ImageXpress high content live imager (Fig. 2*A*). Following imaging, the physical changes of oligodendrocyte cell bodies and processes were analyzed by a neurite outgrowth program (shown in Fig. 2*G*). While the vehicle-treated oligodendrocytes maintained complex morphologies with extensive branching over the course of 24 h, the average complexity of oligodendrocytes treated with dasatinib, quercetin, or D+Q decreased drastically (around 45%) in the 24 h following treatment (Fig. 2*G*), corroborating our previous immunocytochemical complexity analysis (Fig. 2*E*). Interestingly, oligodendrocytes treated with dasatinib, quercetin, or D+Q exhibited widespread process retraction beginning as soon as 20 min after treatment onset (Fig. 2*G* and *SI Appendix*, Fig. S1). These data further suggest that D+Q provokes physical alterations to oligodendrocyte morphology that reduce their ability to extend myelinating processes and hinder active myelination.

Senolytic Treatment Elicits ER Stress and Activates the UPR in Oligodendrocytes. We have shown thus far that D+Q causes demyelination in the brain and hinders oligodendrocyte differentiation and myelination, suggesting that D+Q-induced oligodendrocyte dysfunction leads to demyelination in the brain. To understand how D+Q elicits a change in oligodendrocyte function and find molecular targets of D+Q, we performed total RNA bulk sequencing on RNA isolated from mature oligodendrocytes treated with vehicle, dasatinib, quercetin, or D+Q to assess transcriptomic alterations evoked by D+Q treatment (Fig. 3*A*). Compared to the differentiated controls, oligodendrocytes treated with D+Q, dasatinib, or quercetin differentially expressed 6,191; 5,761; and 3,823 genes, respectively (Fig. 3*B*). Ingenuity pathway analysis (IPA) performed on the bulk RNA sequencing dataset predicted that the top canonical pathways activated by D+Q treatment included "XBP1(S) upregulation of chaperone genes," "macroautophagy," "the unfolded protein response," "autophagy," "ATF6 upregulation of chaperone genes," and "ATF4 gene activation in response to ER stress" (Fig. 3*C*). The top predicted biological processes inhibited following D+Q treatment in oligodendrocytes included eukaryotic initiation, elongation, and termination (Fig. 3*C*). These results indicate that D+Q activates ER stress in oligodendrocytes and suggests that ER stress may mediate the effects of D+Q observed on oligodendrocyte function and thus myelination in the brain.

To further assess the effects of D+Q on oligodendrocyte expression of ER stress-related genes, we analyzed the differential expression of genes known to be associated with the UPR and ER stress in oligodendrocytes treated with vehicle, dasatinib, quercetin, and

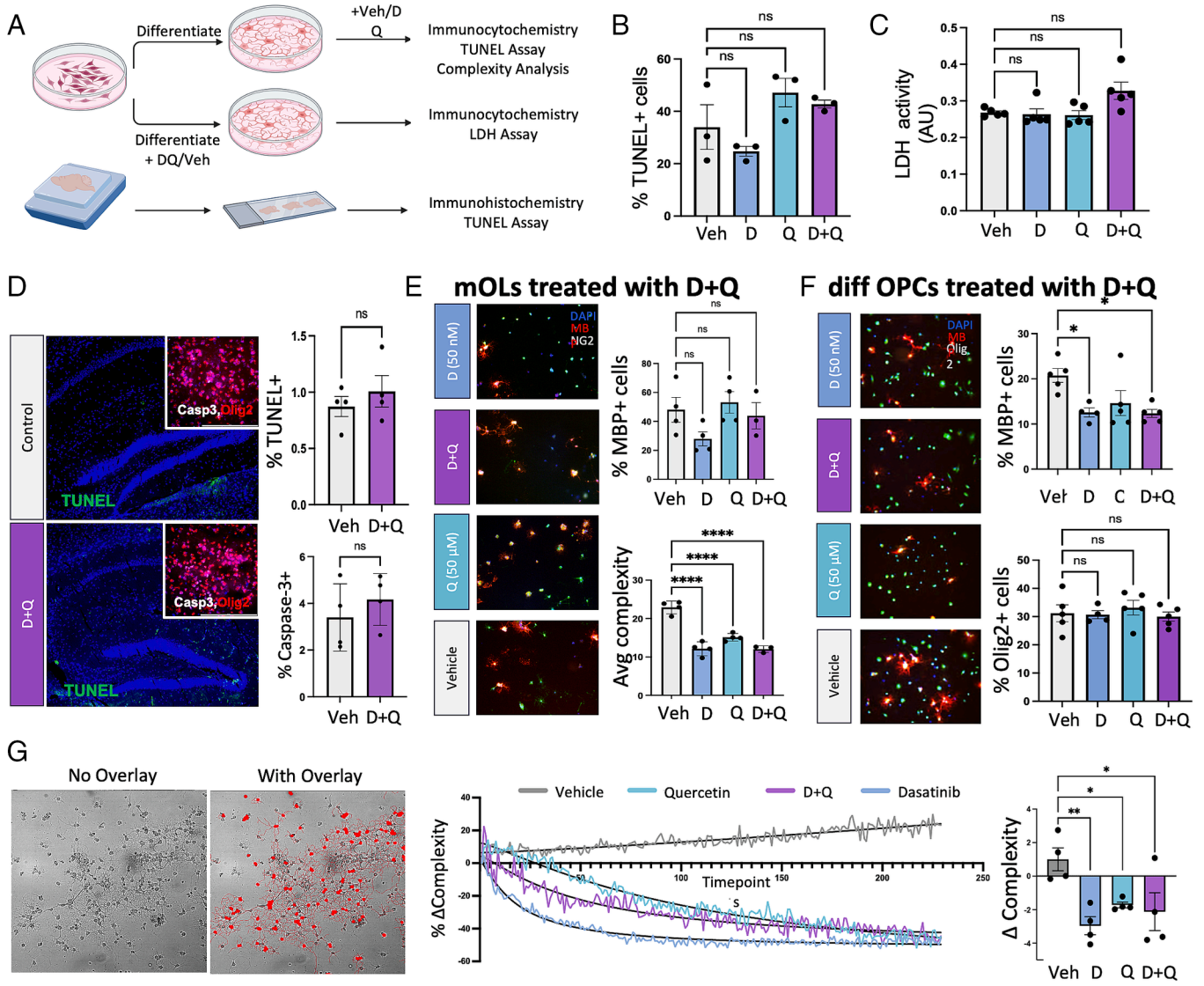

Fig. 2. Senolytic treatment impairs oligodendrocyte differentiation and myelination in vitro. (*A*) Schematic depicting the experimental workflow of treating and analyzing mature oligodendrocytes (as shown in panels *B*, *E*, and *G*) or differentiating oligodendrocyte progenitor cells (OPCs) from primary rat cultures (as shown in panels *C* and *F*) with D+Q as well as the immunohistochemistry performed on formalin-fixed paraffin embedded (FFPE) murine brain sections (as shown in panel *D*). All in vitro studies used cell cultures derived from rats, whereas all in vivo studies used C57Bl6/J mice. (*B*) TUNEL assay performed on mature oligodendrocytes treated with 50 nM dasatinib, 50uM quercetin, or D+Q for 24 h (n = 3; Kruskal–Wallis; $P = 0.0788$) (*C*) LDH assay performed on OPCs treated with D+Q to assess cytotoxic effects of D+Q (n = 5 per treatment group; Kruskal–Wallis; $P = 0.0596$). (*D*) Analysis of cell death in vivo using TUNEL assays and cleaved-caspase 3 (Casp3) immunofluorescence. TUNEL assay and Casp3 staining were performed on FFPE brain sections from mice that had been treated with D+Q or vehicle according to the treatment paradigm described in Fig. 1*A*, and analyzed for cell death using TUNEL (n = 4 per treatment group; Welch's two-tailed *t* test; $P = 0.4479$) and Casp3 staining (*Inset*) (n = 4 per treatment group; Mann–Whitney test; $P = 0.2429$). Representative images of staining are provided and quantification of staining within the hippocampus are shown. Bar graphs represent analysis of TUNEL (*Upper*), and Casp3 staining. (*E*) Immunocytochemical analysis of mature oligodendrocytes treated with D+Q for 24 h to evaluate the effect of D+Q on oligodendrocyte myelination in vitro using MBP (red), Olig2 (green), and DAPI. The percent of MBP+ cells (n = 4 per treatment group; One-way ANOVA; $P = 0.1447$) and the average cellular complexity (n = 4; One-way ANOVA; $P < 0.0001$ where $^{****}P < 0.0001$) was compared between treatment groups. (*F*) Immunocytochemical analysis of OPCs treated with D+Q in differentiation media for 72 h to assess the effects of D+Q on the maturation and differentiation of OPCs in vitro. OPCs were stained for myelin marker MBP (red), DAPI, and pan-oligodendrocyte marker Olig2 (green). The percent of MBP+ cells (n = 5 per treatment group, except n = 4 for Q; One-way ANOVA; $P < 0.05$ where $^{*}P < 0.05$) and percent of Olig2+ cells (n = 5 per treatment group, except n = 4 for Q; One-way ANOVA; $P = 0.7881$) were compared between treatment groups. (*G*) Sholl analysis on mature oligodendrocytes treated with D+Q for 24 h to evaluate the effects of D+Q on the morphology and complexity of oligodendrocytes in vitro. The graph displays the change in average complexity of oligodendrocytes over 24 h, starting at the onset of treatment (tp 0), where positive and negative *y*-values indicate increases and decreases in complexity compared to the initial complexity of the oligodendrocytes, respectively. The datasets were fitted with nonlinear regressions. The overlay (*Left* picture) depicts an example mask drawn by the neurite outgrowth program of the Metaxpress software on one image of oligodendrocytes (*Right* picture) that was used to analyze the oligodendrocyte processes and cell bodies through Sholl analysis. The line graph depicts the average change in complexity over time throughout 24 h of treatments (5 min/timepoint) and the bar graph represents the total change in average complexity per treatment group (n = 4 per treatment group; one-way ANOVA $P < 0.05$, where $^{*}P < 0.05$ and $^{**}P < 0.01$).

D+Q using the bulk RNA sequencing dataset. We found that key genes involved in the UPR were significantly upregulated by oligodendrocytes treated with D+Q, including heat shock 70 kDa protein 5 (*Hspa5*/*Bip*), X-box binding protein 1 (*Xbp1*), activating transcription factor 4 (*Atf4*), and DNA damage-inducible transcript 3 (*Ddit3*/*Chop*), tribbles pseudokinase 3 (*Trib3*), and asparagine synthetase (*Asns*) (Fig. 3*G*), reinforcing IPA predictions that D+Q-treated oligodendrocytes activated ER stress pathways. Interestingly, the bulk sequencing data revealed that gene targets downstream of ATF4 were particularly enriched in D+Q treated oligodendrocytes, indicating that the PERK-dependent pathway was specifically upregulated (Fig. 3*H*). These data support the

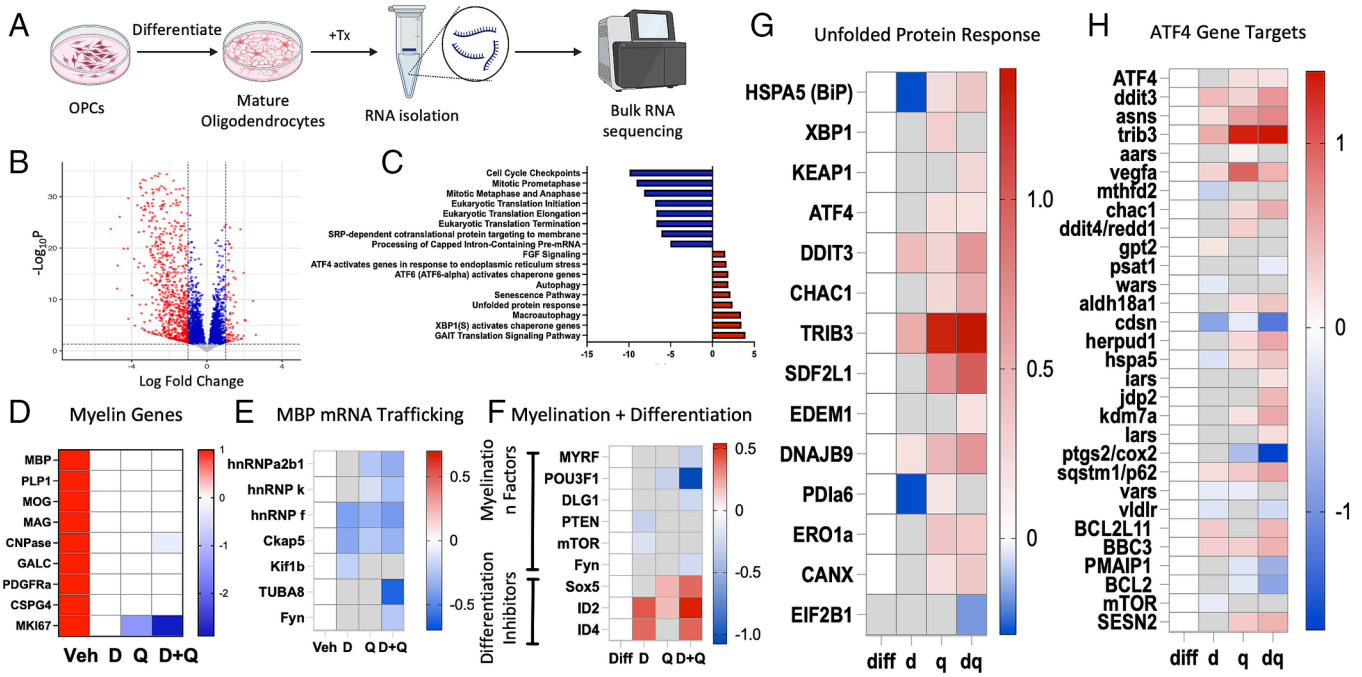

Fig. 3. D+Q caused a shift in oligodendrocyte transcription that opposed myelination and upregulated the unfolded protein response. (*A*) Schematic depicting the experimental design. RNA from oligodendrocytes treated with D+Q for 24 was isolated from each sample and sequenced. (*B*) Volcano plot displaying the distribution of differentially expressed genes according to log2fold change and −log10 *P*-value. (*C*) Graph displaying the most activated and inhibited biological processes and pathways in oligodendrocytes following D+Q treatment according to IPA predictions based on the bulk RNA sequencing dataset (*D*–*H*) Heat maps displaying the differentially expressed genes from oligodendrocytes treated with dasatinib (D), quercetin (Q), and D+Q compared to controls (Diff) involved in making myelin and development (*D*), MBP mRNA trafficking (*E*), oligodendrocyte differentiation and myelination (*F*), the unfolded protein response (*G*), and downstream transcriptional targets of ATF4 (*H*).

hypothesis that D+Q treatment upregulates ER stress and the unfolded protein response in oligodendrocytes and provides a potential mechanism through which D+Q causes dysfunction in oligodendrocytes.

To assess whether the UPR was upregulated in the brain following D+Q treatment, we stained brain sections from D+Q-treated and vehicle-treated aged mice with anti-ATF4, anti-XBP1, and anti-Olig2 antibodies to visualize ATF4 and XBP1 expression in oligodendrocytes (Fig. 4*A*). We found that oligodendrocytes significantly upregulated ATF4 and XBP1 in the rostral CC (Fig. 4*B*), validating our in vitro sequencing data suggesting that D+Q treatment upregulates the UPR in oligodendrocytes. Notably, the rostrum also exhibited rampant demyelination (Fig. 1*B*). This supports the hypothesis that D+Q-induced oligodendrocyte ER stress leads to demyelination in the brain, though further studies are necessary to validate this hypothesis.

Senolytic Treatment Reduces Expression of Myelination Factors But Maintains Mature Transcriptional Profile in Oligodendrocytes. We also assessed the effect of D+Q treatment on the expression of myelination-related genes and maturation markers. Examination of the bulk RNA sequencing dataset revealed that oligodendrocytes treated with D+Q downregulated genes that promote myelination like FYN proto-oncogene (*Fyn*) and myelin regulatory factor (*Myrf*) (Fig. 3*F*). We noted that inhibitors of terminal oligodendrocyte differentiation SRY-Box Transcription Factor 5 (*Sox5*), Inhibitor of DNA Binding 2 (*Id2*), and Inhibitor of DNA Binding 4 (*Id4*) (33–35) were upregulated in oligodendrocytes when treated with D+Q compared to controls (Fig. 3*F*). Interestingly, D+Q-treated oligodendrocytes also downregulated the expression of genes involved in the transportation of MBP mRNA, including genes of critical RNA binding proteins, motor proteins, and microtubules like heterogeneous nuclear ribonucleoprotein A2/B1 (*hnRNPa2b1*), K (*hnRNPk*), and f (*hnRNPf*), cytoskeleton-associated protein 5 (*Ckap5*/Tog), kinesin family member 1B (*Kif1b*), and tubulin alpha 8 (*Tuba8*) (Fig. 3*E*), suggesting a possible impact on MBP mRNA transport as well within the mature oligodendrocytes. Together, these data suggest that D+Q inhibits several factors and processes involved in myelination, further supporting the hypothesis that D+Q treatment impairs oligodendrocyte function, leading to myelination failure.

As myelination-related genes are downregulated in D+Q-treated oligodendrocytes, one might expect to observe a similar decrease in myelin-related genes and maturation markers. So, we evaluated differences in expression of genes encoding myelin proteins, markers of mature oligodendrocytes, and OPCs between D+Q-treated oligodendrocytes and mature vehicle-treated controls. We found that D+Q-treated oligodendrocytes downregulated CNP, but did not differentially express other mature markers including MBP, proteolipid protein 1 (PLP1), myelin oligodendrocyte glycoprotein (MOG), or myelin-associated glycoprotein (MAG) (Fig. 3*D*). D+Q-treated oligodendrocytes also did not differentially express OPC markers like platelet-derived growth factor receptor alpha (PDGRFa) and chondroitin sulfate proteoglycan 4 (CSPG4) (Fig. 3*D*). Furthermore, D+Q-treated oligodendrocytes significantly downregulated marker of proliferation Ki-67 (Mki67) (Fig. 3*D*). Together, these findings indicate that D+Q-treated oligodendrocytes were transcriptionally mature and contradicts the hypothesis that D+Q causes a transcriptional reversion of oligodendrocytes to an immature state.

Discussion

This study showed that senolytic treatment induced demyelination of the brains of naïve young and aged C57BL6/J mice, specifically in the rostral corpus callosum (Fig. 1), without inducing significant

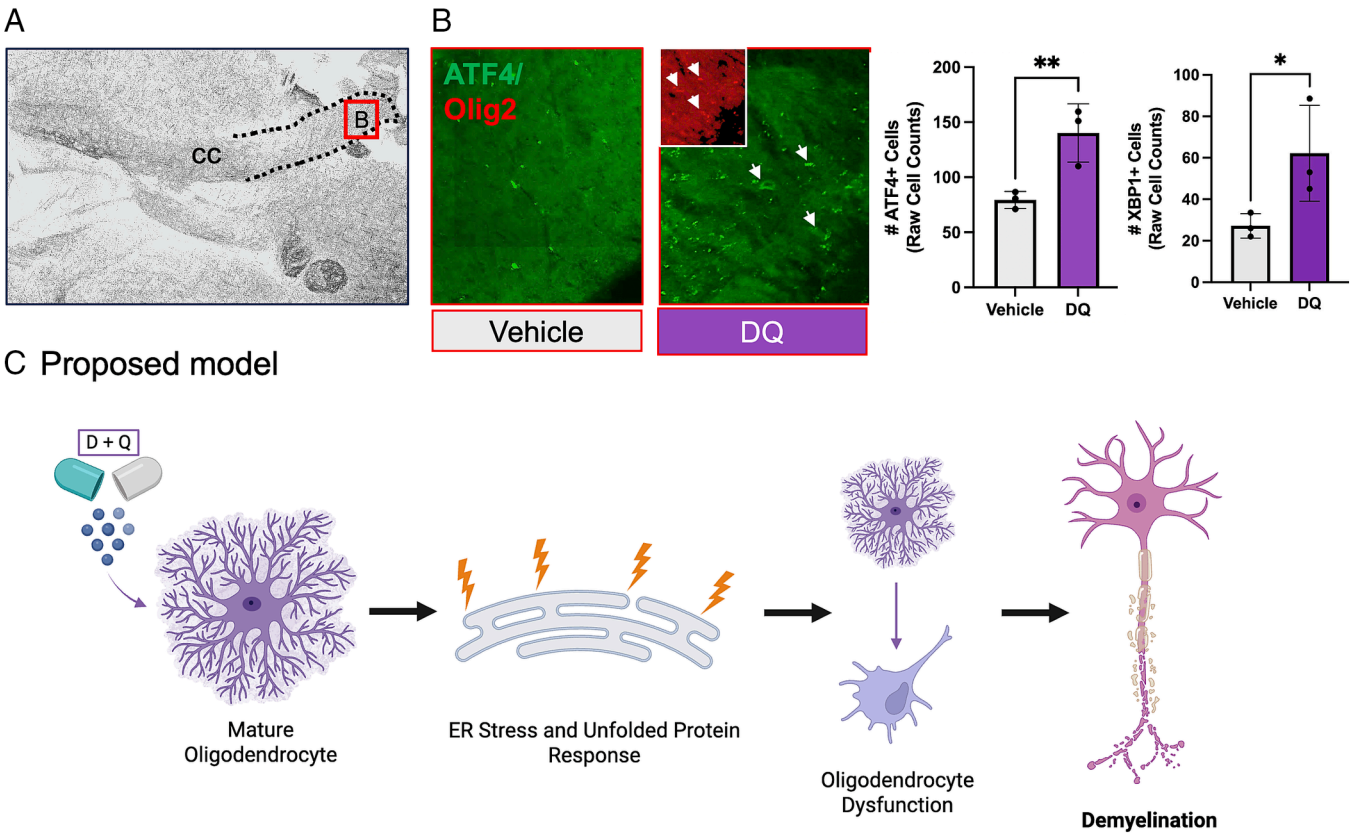

Fig. 4. D+Q-induced ER stress evokes the unfolded protein response in oligodendrocytes which leads to demyelination in the brain. (*A*) Black and white image depicting the corpus callosum (CC) and the rostral region of the CC (outlined) analyzed in C57Bl6/J mice shown in (*B*). The red box depicts the area represented by the images and analyzed in (*B*). (*B*) ATF4 staining (Green) and Olig2 (*Inset*) of the rostral corpus callosum (red box in (*A*)). Arrows point to representative Olig2+ ATF4+ cells. Quantification of ATF4+/Olig2+ cells and Xbp1+/Olig2+ cells in D+Q or vehicle-treated mice were compared (n = 3 mice per treatment group; unpaired *t* test; where $*P < 0.032$, $**P < 0.01$). (*C*) Schematic representing the proposed hypothesis wherein D+Q activates the UPR in oligodendrocytes, causing dysfunction and myelination failure, leading to demyelination in the brain.

cell death or cytotoxicity in the brain compared to controls (Fig. 2). To better understand how D+Q caused demyelination and oligodendrocyte dysfunction, we treated primary cultures of oligodendrocytes and OPCs from rats with D+Q. TUNEL and LDH assays performed on mature oligodendrocytes treated with D+Q validated our findings in vivo, showing no significant difference in cell death compared to vehicle-treated controls (Fig. 2). Using both time-lapse video microscopy and immunocytochemistry, we also found that D+Q-treated oligodendrocytes exhibited significant loss of complexity over 24 h while OPCs failed to differentiate (Fig. 2). These data suggest that D+Q impairs the ability of oligodendrocytes to maintain a branching network of outgrowths needed for myelination and prevents OPC differentiation. Together, the absence of functioning oligodendrocytes and the failure of OPCs to replace them may be sufficient to produce demyelination in the brain. This idea is consistent with the notion that dysfunctional oligodendrocytes and quiescent OPCs contribute to demyelination and remyelination failure in multiple sclerosis (36–39). We propose that the findings herein shed light on possible mechanisms by which this may occur.

One key finding of this study was that D+Q upregulated ER stress and the UPR in oligodendrocytes, suggesting a role for the UPR in D+Q-induced oligodendrocyte dysfunction and demyelination. We showed that D+Q upregulated the expression key UPR markers like ATF4, XBP1, and HSPA5, indicating that D+Q induces ER stress and the UPR in oligodendrocytes. IPA also predicted that the UPR was activated in D+Q-treated oligodendrocytes. Typically, acute activation of the UPR is considered cytoprotective as it temporarily halts protein synthesis to correct protein folding in the ER. However, the global translation block initiated by the phosphorylation of eukaryotic translation initiation factor 2A (eif2a) reduces the capacity of oligodendrocytes to produce the extensive volume of proteins required to sustain active myelination and differentiation (40). In turn, this could result in a loss of compact myelination, process retraction, and reduced maturation of OPCs, which together contribute to demyelination and failed remyelination in the brain (Fig. 4, schematic). Previous studies investigating the effects of ER stress and the UPR on oligodendrocyte function and myelination corroborate this idea. While a few studies have shown that activation of the UPR improves oligodendrocyte function and myelination (41), most studies have reported that activation of ER stress and the UPR exacerbates oligodendrocyte dysfunction and myelination failure (40, 42–44). This observation is consistent with prior work reporting that stimulation of the UPR in human derived oligodendrocytes resulted in process retraction, and that oligodendrocyte process extension could be restored during stressful conditions by blocking the UPR (45). Evidently, the activation of the UPR in oligodendrocytes as a result of D+Q treatment likely contributes to oligodendrocyte dysfunction and myelination defects observed in this study. Moreover, the similarity of the effects observed through UPR stimulation and ER stress in previous studies further suggests that ER stress may mediate the effects of D+Q treatment on oligodendrocyte function.

Another critical finding of this study was the observation that D+Q evoked demyelination without oligodendrocyte death. Prior studies have shown that fibroblast growth factor 2 (fgf2) can induce loss of a mature phenotype in oligodendrocytes, resulting in a more

immature oligodendrocyte cell state (46, 47). Interestingly, FGF signaling was predicted by IPA to be strongly activated by D+Q treatment in oligodendrocytes (Fig. 3). As initial evidence in vivo shows D+Q caused demyelination without cell death (Figs. 1 and 2), it would be reasonable to suggest that D+Q may be similarly inducing a less mature oligodendrocyte cell state through FGF signaling. Moreover, our live imaging data show oligodendrocytes losing complexity, returning to simplified morphologies characteristic of immature oligodendrocytes (Fig. 2). Interestingly, there was no significant difference in the expression of mature and immature oligodendrocyte markers following D+Q treatment compared to controls (Fig. 3), suggesting that D+Q-treated oligodendrocytes were transcriptionally like mature oligodendrocytes despite acquiring a less mature morphology. Immunocytochemistry staining of mature oligodendrocytes treated with vehicle or D+Q supports this idea, indicating that D+Q treatment had no impact on the proportion of MBP+ or NG2+ oligodendrocytes. Furthermore, PCA analysis determined that D+Q-treated oligodendrocytes were more like vehicle-treated mature oligodendrocytes than to OPCs, suggesting a loss of myelinating function rather than a reversion of maturity per se (*SI Appendix*, Fig. S2). Thus, these data suggest that a similar mechanism may induce D+Q-induced oligodendrocyte dysfunction and demyelination in this study.

An important application of this work is the potential insight it provides into oligodendrocyte biology, and how oligodendrocytes function under stress. The upregulation of ER stress and UPR in oligodendrocytes caused by D+Q treatment mirrors stressed oligodendrocytes observed in the MS brain. Previous studies have broadly implicated ER stress in MS (40, 43, 45, 48, 49). For example, two groups separately found that protein and mRNA of UPR markers XBP1, DDIT3, HSPA5, and ATF4 were upregulated in acute MS lesions compared to non-MS control tissue and MS normal appearing white matter (50, 51). Absinta et al. further indicated that a distinct population of stressed oligodendrocytes which upregulate the UPR are elevated in demyelinated brain lesions of patients with progressive MS compared to control samples (52). These data suggest that ER stress in oligodendrocytes contributes to demyelination and further corroborate the hypothesis that D+Q-induced UPR activation contributes to oligodendrocyte dysfunction and demyelination. Moreover, the similarities between oligodendrocytes treated with D+Q and the stressed oligodendrocytes outlined by Absinta et al. offers the potential to model pathological features of oligodendrocytes observed in MS that contribute to demyelination and disease progression.

It is also worth noting that demyelination resulting from chemotherapy has been associated with diminished cognitive function, often referred to as "chemo-brain." In the context of this study, although not tested, the effect of D+Q on the rostral corpus callosum would align with a potential impact on cognition. Hence, an outcome of this study is also the potential susceptibility of specific myelinated domains to chemotherapeutics. Whereas in a prior study it was found that methotrexate could negatively affect myelination in the same brain area (53). The reason(s) why specifically this aspect of the corpus callosum would be differentially affected is presently unclear. Our findings on the effect of dasatinib are entirely consistent with this previous study and provide a consensus that this specific region of the corpus callosum has a high susceptibility to demyelination in response to chemotherapeutics.

Our timelapse video imaging of oligodendrocytes in vitro post-D+Q treatment exhibit retraction of presumptive myelinating processes, which provides a compelling explanation for the observed demyelination without cell death in vivo. While we have not performed fate mapping studies in this study, future experiments to explore this notion may test this possibility. Nevertheless, our RNAseq data from D+Q treated oligodendrocytes suggest that this treatment has a significant impact on gene expression. Notable among these changes in gene expression was the downregulation of genes encoding mRNA transport proteins while expression of myelin genes appeared stable. It is important to note that the mRNA for myelin basic protein, which encodes for a key myelin protein, is not translated in the cell body but is transported to the cellular extensions for local translation. These data provide a possible model in which ER stress/UPR may affect the myelinating potential of oligodendrocytes through disruption of critical mRNA transport, which could initiate retraction of processes (in vitro) and loss of compact myelination (in vivo). Hence, these data provide a model in which perturbation of myelin homeostasis initiates oligodendrocyte dysfunction resulting in reduced compact myelination of axons (Fig. 4).

In summary, we have found that D+Q causes demyelination in the brain, likely through oligodendrocyte dysfunction resulting from ER stress. Due to the similarities between oligodendrocytes treated with D+Q and those residing in demyelinated MS lesions, D+Q treatment offers a potential method to model an aspect of oligodendrocyte dysfunction relevant to MS in vitro. Therefore, understanding the mechanism(s) by which D+Q affects oligodendrocytes, and potential remedies to this, could provide beneficial insight into some of the pathological features contributing to disease progression in MS. Moreover, the potential implications of these findings for D+Q treatment on myelination in the brain in a range of senescence-associated disorders has not been explored and may warrant further investigation.

Materials and Methods

In Vivo D+Q Treatment. Young (3 mo) and aged (22 mo) wildtype C57Bl6/J mice (JAX strain #000663) were orally gavaged with either vehicle (10% ethanol, 30% PEG-400, and 60% Phosal-50PG) or senolytic cocktail (D+Q). Dasatinib and quercetin were administered at a concentration of 5 mg/kg and 50 mg/kg, respectively. Both young and aged mice were gavaged with D+Q once every other day during the first and third week of treatment. No treatments were administered during weeks 2 and 4, and animals were further processed for TEM and immunohistochemistry (IHC) at the end of week 4.

Histology and Immunohistochemistry (IHC). D+Q- and vehicle-treated mice, aged and young, were perfused with 1× PBS. The brains were dissected, split down the midline using a razor blade, and placed in tissue cassettes. The samples were immersed in formalin overnight at 4 °C. The samples were removed from the formalin and placed sequentially in 70%, 90%, 95%, and 100% ethanol each for 1 h. The samples were moved to a bottle of 1:1 xylene and ethanol for 10 min and then placed in xylene for 1 h. To gradually replace the xylene with paraffin, the samples were placed in a melted 1:1 xylene and paraffin mixture overnight at room temperature and then immersed in paraffin maintained at 68 °C using a water bath for 3 h, replacing the paraffin every hour. Following paraffin infiltration, the samples were embedded and sliced into 8 μm sections on polarized slides. D+Q-treated, vehicle-treated, and cuprizone-treated (+control) mouse slides were heated at 60 °C for 30 min prior to deparaffinization. The slides were deparaffinized in three changes of xylene for 5 min each and rehydrated in a decreasing gradient of ethanol dilutions in tap water. Then, samples were microwaved in 0.01 M citric acid buffer (pH = 6) for 30 min and allowed to cool. A hydrophobic barrier was drawn around the samples using a pap pen before incubating the slides in blocking buffer (5% NGS in PBST) for 1 h at RT. Samples were washed three times in 1× PBS for 5 min and then incubated in primary antibodies diluted in 2% NGS in PBST (mouse anti-ATF4 1:250, Santa Cruz; goat anti-Olig2 1:350, Santa Cruz; rabbit anti-cleaved caspase 3 1:100, Cell Signaling) for 1.5 h at 37 °C in a humidity chamber. Slides were washed three more times in 1x PBS and incubated in secondary antibodies diluted in 1× PBS [Gt anti-Rb IgG (H+L), AF 488 1:500, ThermoFisher; Donkey anti-Gt IgG (H+L), AF 633 1:250, ThermoFisher; Gt anti-Ms 488 1:250, Invitrogen] for 1 h at room temperature in the dark. After incubation, the slides were washed three times with 1× PBS and

then mounted with prolong gold DAPI antifade mounting media (Invitrogen). Slides were imaged on an inverted IX71 olympus microscope.

TUNEL Assays. TUNEL assays were performed according to the protocol outlined by Cell Signaling in the TUNEL Assay Kit (488 nm). D+Q-treated, vehicle-treated, and cuprizone-treated (+control) mouse brain samples were deparaffinized in three changes of xylene for 5 min each and rehydrated in a decreasing gradient of ethanol dilutions in tap water. Then, samples were microwaved in 0.01 M citric acid buffer (pH = 6) for 30 min and allowed to cool. A hydrophobic barrier was drawn around the samples using a pap pen before incubating the slides in blocking buffer for 1 h at RT. Samples were washed twice in PBS for 5 min and then incubated with TUNEL equilibrium buffer for 5 min at RT. Equilibrium buffer was removed and 50 μL of TdT enzyme diluted 1:50 in TUNEL reaction buffer was added to each sample for 1.5 h at 37 °C, protected from light. Slides were washed three times in PBS–TB and mounted using prolong gold DAPI antifade mounting media (Invitrogen). Slides were imaged using an inverted IX71 Olympus microscope.

TUNEL assays performed on cultured oligodendrocytes followed the procedure outlined by Cell Signaling in the TUNEL Assay Kit (488 nm). Mature oligodendrocytes were treated with D+Q for 24 h and then fixed with 4% PFA at RT for 20 min. The fixed cells were washed with PBS twice for 5 min each, permeabilized with PBS–TB for 30 min at RT, and washed twice more for 5 min. The cells were incubated with 100 μL TUNEL equilibrium buffer for 5 min at RT and subsequently incubated with 50 μL of TdT enzyme diluted 1:50 in TUNEL reaction buffer was added to each sample for 1.5 h at 37 °C, protected from light. The cells were washed three times with PBS–TB for 5 min and then mounted onto slides using prolong gold DAPI antifade mounting media (Invitrogen). Slides were imaged using an inverted IX71 Olympus microscope.

Transmission Electron Microscopy. Mice treated with vehicle or D+Q were anesthetized with isoflurane and perfused with 10 mL of 1× PBS followed by 10 mL of fixative (2% PFA and 2.5% glutaraldehyde in 0.1 M cacodylate buffer). To ensure proper fixation, the brains were removed 10 min after perfusion and immersed in fixative for 1 h at room temperature. Since we aimed to capture myelination in the brain, we isolated a cross-section of the corpus callosum from each brain using a razor blade and brain matrix. The samples were washed at least five times in 0.1 M cacodylate buffer. Subsequently, the samples were postfixed in cacodylate buffer containing 1% osmium tetroxide (OsO4) and 0.8% ferricyanide for 1 h at room temperature and washed in diH2O five times for 5 min. 1% uranyl acetate in diH2O was used to stain the samples for 1 h at room temperature. Following four additional rinses with diH_2O, the samples were gradually dehydrated in increasing concentrations of ethanol (one rinse for 10 min in 50% EtOH, 75% EtOH, 95% EtOH, followed by 3 10-min rinses in 100% EtOH). Samples were rinsed in propylene oxide (PO) twice for 5 min. The samples were added to a 1:1 mixture of PO and Poly/Bed812 resin for 1 h at room temperature followed by 2 h in a 1:3 PO and resin solution. The samples were placed in 100% resin overnight at room temperature. The following day, the samples were transferred into fresh resin in a silicon mold and heated to 60 °C for at least 24 h. Ultrathin (0.1 μm) sections were cut from each sample block and imaged using a transmission electron microscope (80 kV, 5,000× magnification). Images were analyzed using the G-ratio plugin available through ImageJ, created by the Naves lab, to quantify myelination in the brain. In the aged mice, 2000 total axons were analyzed from three separate mice per treatment group. In young mice, 1,500 total axons were analyzed from three separate mice per treatment group. This experiment was replicated three times, though the data are representative of only one experiment.

Rat OPC Primary Culture and Plating. Rat OPCs were dissected from the cortices of rat pups (postnatal day 0 to 3). The meninges and hippocampi were removed from the rat brains, and the cortices were homogenized using autoclaved microdissection scissors and a heat-sterilized Pasteur pipette. The homogenate was centrifuged at 1,800 rpm for 10 min, resuspended in mixed glia culture media (DMEM/F12 + 10% FBS + 1% penicillin-streptomycin), and plated on poly-l-lysine (0.3 mg/mL) coated flasks. The flasks were incubated for 10 d or until the cell layer was confluent, changing the media every 4 d, after which the flasks were shaken at 55 rpm for 1.5 h at 37 °C. The media were aspirated to remove microglia and 10 mL of fresh, prewarmed mixed glia media (see *SI Appendix*, Table S1) was added to each flask. The flasks were incubated (37 °C, 5% CO_2) for 3 h and shaken overnight at 200 rpm, 37 °C. The following morning, the media were collected into a 50 mL conical tube using serological pipettes and centrifuged at 1,800 rpm for 7 min at room temperature (RT). The media were carefully aspirated to not disturb the pellet. The pellet was resuspended in 10 mL of prewarmed mixed glia media, placed onto a nontissue culture treated petri dish, and incubated for 1.5 h. To avoid cell clumping and OPCs adhering to the plate, the petri dish was gently swirled in a figure-eight motion periodically throughout the incubation. The media were collected after swirling the petri dish and used to gently rinse the petri dish 3 times before finally transferring the media to a 50 mL conical tube. The cells were centrifuged at 1,800 rpm for 7 min at RT. Subsequently, the cell media were aspirated, and the cell pellet resuspended in 1 mL OPC proliferation media (see *SI Appendix*, Table S1). The cell concentration was determined using an automated cell counter (BioRad). The cell pellet was further diluted in proliferation media to achieve a final concentration of around 200,000 cells/ml and transferred to a new 50 ml conical through a 40 μm cell strainer (Fisher, 22363547) to remove cell clumps and debris. 500 μL of the cell homogenate were seeded onto poly-l-lysine coated glass coverslips within a 24-well plate (CellTreat) at a density of 50,000 cells/cm^2 and gently swirled to ensure even distribution of cells within each well. Once plated, the cells were incubated overnight, after which the proliferation media were replaced with 500 μl of fresh, prewarmed proliferation media.

All cells were plated on 12 mm glass Coverslips (Platinum Line). The coverslips were washed with 1 N HCl for 30 min in a large petri dish and then rinsed 3 times with sterile water. The coverslips were then washed with 95% ethanol for 3 min and allowed to air dry. Once dry, the coverslips were placed on 70 μL droplets of poly-l-lysine (Gibco) and incubated for at least 3 h. Before cells were plated, coverslips were placed into wells adhesive-side up and washed 3 times with sterile water.

Immunocytochemistry. OPCs were plated in a 24-well plate at a density of 50,000 cells/cm^2 (100,000 cells in 500 μL in a well with an area of 2 cm^2) in 500 μL of proliferation media for 24 h. The media was replaced with 500 μL of fresh, warmed proliferation media, and the cells were incubated for 3 d, allowing the OPCs to adhere to the coverslips. To differentiate the OPCs into mature oligodendrocytes (mOLs), the media was subsequently changed to differentiation media (*SI Appendix*, Table S1) for 72 h. Following differentiation, the cells were treated with D, Q, D+Q, or vehicle for 24 h. Control wells contained only differentiation media. The media was removed using a p1000 pipette and the cells were fixed with 4% PFA (Sigma Aldrich) for 20 min at RT. The wells were washed three times with PBS for 5 min each and subsequently blocked in 5% normal goat serum diluted in PBS-T for 1 h at RT. The 5% NGS was removed and the wells were incubated with anti-MBP (1:250, Millipore), anti-NG2 (1:250, Millipore), or anti-Olig2 (1:250, Abcam) antisera diluted in 2% NGS in PBS-T for 1.5 h at RT. The wells were washed with PBS three times with continuous slight agitation for 5 min per wash. The cells were incubated with alexa-fluor conjugated secondary antibodies (AF 488 or AF 594, 1:250; ThermoFisher) diluted in PBS for 1 h at RT in the dark. The wells were washed with PBS for 5 min three times. Coverslips were mounted onto slides with prolong gold DAPI antifade mounting media (Invitrogen) and visualized with an inverted Olympus IX71 microscope. See *SI Appendix*, Table S2 for a full list of antibodies and chemicals used in this study.

RNA Isolation and Bulk RNA Sequencing. RNA isolation was performed according to the Sigma Aldrich TRI reagent protocol. Oligodendrocyte progenitor cells were differentiated for 72 h and then treated with vehicle, D, Q, and D+Q for 24 h in oligodendrocyte base media. The media was removed and 0.5 mL of Trisol (Sigma Aldrich) was added to each well. The bottoms of the wells were scraped using small cell lifters to detach the oligodendrocyte cell layer. The lysate was sheared and homogenized using 1 ml syringes with 26-gauge needles and transferred to 1.5 mL Eppendorf tubes. The samples were spun at 12,000× g for 10 min at 4 °C and the supernatant was transferred to fresh 1.5 mL tubes. Chloroform (100 μL) was added to each sample. The samples were vigorously shaken for 15 s, left at RT for 15 min, and then centrifuged at 12,000× g for 10 min at 4 °C. The clear, aqueous phase was removed and transferred to new 1.5 mL tubes. 2-propanol (250 μL) was added to the aqueous homogenate containing RNA and left at RT for 10 min. The samples were centrifuged again at 12,000× g for 10 min at 4 °C, precipitating the RNA at the bottom of each tube. The supernatant was carefully removed, leaving the pellet undisturbed, and 500 μL of 70% ethanol was added to each tube. The samples were vortexed

and then centrifuged at 12,000× g for 5 min at 4 °C. The supernatant was once again removed, washed with 70% ethanol and then centrifuged 12,000× g for 5 min at 4 °C. Most of the supernatant was removed using a p200 pipette and then the samples were air-dried, though ensuring to not completely dry out the pellet. The RNA pellet was resuspended in 20 μL of RNase- and DNase-free water and then stored at −20 °C.

RNA quality checks, bulk RNA sequencing, and bioinformatics were performed by the Center for Genome Innovation (CGI) and the Computational Biology Core (CBC) of the University of Connecticut Storrs. Samples were grouped by treatment condition and analyzed in respect to vehicle-treated mature oligodendrocytes.

Time-Lapse Imaging and Complexity Analysis. Oligodendrocyte progenitor cells were plated in proliferation media in a 24-well glass-bottom plate (MatTek P24G-1-5-13-F) according to the protocols described above and then differentiated for 72 h. The media was replaced with oligodendrocyte base media (no PDGFA, FGF2, or T3) supplemented with vehicle, D, Q, D+Q, or vehicle. The cells were then incubated in an ImageXpress Confocal HT.ai high content imaged equipped to maintain environmental controls (Molecular Devices) for 24 h, throughout which MetaXpress, an imaging and analysis software by Molecular Devices, captured four nonadjacent 10× brightfield images of each well every 5 min. The neurite outgrowth program on the MetaXpress software overlaid every image with a mask marking cell bodies and outgrowths using localized pixel intensity thresholds. The neurite outgrowth program subsequently quantified the average complexity of the oligodendrocytes using a Sholl analysis-like approach. The mean complexity of oligodendrocytes grown under experimental conditions were compared to that of vehicle-treated oligodendrocytes.

MBP immunofluorescence complexity analysis. Representative sites of mature oligodendrocyte cultures stained with MBP, NG2, and DAPI, and treated with either vehicle, dasatinib, quercetin, or D+Q were imaged 24 h after treatment. The treatment paradigm and immunocytochemistry protocol used were consistent with those described in these methods. Through ImageJ, we created a composite image overlaying both the MBP (AF 594) and NG2 (AF 488) channels and made a binary mask of the cell bodies and processes. These images were further filtered to remove any background signal. These binary images, representing the cells of their corresponding image, were run-through the Sholl analysis program within ImageJ. This program functions similarly to the neurite outgrowth program described in this section, where concentric rings are overlaid onto each image and the total intersections between the rings and a cell are counted. The output of this program is a number representing the total intersections between all the cells of one image and the concentric rings. To control for variance in cell counts per image which heavily influences the total number of intersections counted by the program, the total number of intersections for each image was divided by the number of cells within the corresponding image. Cells were counted using the DAPI stain. This function provides a measure of the average number of intersections between each cell and the concentric rings, which we refer to as the mean complexity of a cell. Each data point presented in Fig. 2*F* represents the averaged mean complexity of a cell within a biological replicate of a single treatment group, which we refer to as average complexity. The average complexity of cells was compared among treatment groups in Fig. 2*F*.

Data, Materials, and Software Availability. All study data are included in the article and/or supporting information.

Author affiliations: [a]Department of Neuroscience, University of Connecticut School of Medicine, Farmington, CT 06030; [b]Mandell Center for Multiple Sclerosis, Mount Sinai Rehabilitation Hospital, Trinity Health of New England, Hartford, CT 06112; [c]Department of Rehabilitative Medicine, Frank H. Netter School of Medicine at Quinnipiac University, North Haven, CT 06518; [d]Center for Regenerative Medicine and Skeletal Development, University of Connecticut School of Dental Medicine, Farmington, CT 06030; [e]Center on Aging, University of Connecticut School of Medicine, Farmington, CT 06030; and [f]Department of Immunology, University of Connecticut School of Medicine, Farmington, CT 06030

Author contributions: E. R. Lombardo, R.S.P., V.M.S., J.M.B., and S.J.C. designed research; E. R. Lombardo, R.S.P., J.T.L., Z.D., A.L., L.E.P., E. R. Lavoie, V.M.S., J.M.B., and S.J.C. performed research; E. R. Lombardo, R.S.P., Z.D., E. R. Lavoie, and S.J.C. analyzed data; and E. R. Lombardo and S.J.C. wrote the paper.

1. J. S. Graves *et al.*, Ageing and multiple sclerosis. *Lancet Neurol.* **22**, 66–77 (2023).
2. J. Z. Guan *et al.*, Patients with multiple sclerosis show increased oxidative stress markers and somatic telomere length shortening. *Mol. Cell. Biochem.* **400**, 183–187 (2015).
3. K. M. Krysko *et al.*, Telomere length is associated with disability progression in multiple sclerosis. *Ann. Neurol.* **86**, 671–682 (2019).
4. B. Stankoff *et al.*, Age at onset determines the occurrence of the progressive phase of multiple sclerosis. *Neurology* **68**, 779–781 (2007).
5. A. Scalfari, A. Neuhaus, M. Daumer, G. C. Ebers, P. A. Muraro, Age and disability accumulation in multiple sclerosis. *Neurology* **77**, 1246–1252 (2011).
6. A. M. Weideman, M. A. Tapia-Maltos, K. Johnson, M. Greenwood, B. Bielekova, Meta-analysis of the age-dependent efficacy of multiple sclerosis treatments. *Front. Neurol.* **8**, 577 (2017).
7. A. M. Nicaise *et al.*, Cellular senescence in progenitor cells contributes to diminished remyelination potential in progressive multiple sclerosis. *Proc. Natl. Acad. Sci. U.S.A.* **116**, 9030–9039 (2019).
8. J. W. Shay, W. E. Wright, Hayflick, his limit, and cellular ageing. *Nat. Rev. Mol. Cell Biol.* **1**, 72–76 (2000).
9. L. Hayflick, P. S. Moorhead, The serial cultivation of human diploid cell strains. *Exp. Cell Res.* **25**, 585–621 (1961).
10. M. E. Rouillard *et al.*, The cellular senescence factor extracellular HMGB1 directly inhibits oligodendrocyte progenitor cell differentiation and impairs CNS remyelination. *Front. Cell. Neurosci.* **16**, 833186 (2022).
11. N. Kudlova, J. B. De Sanctis, M. Hajduch, Cellular senescence: Molecular targets, biomarkers, and senolytic drugs. *Int. J. Mol. Sci.* **23**, 4168 (2022).
12. S. Maurer, V. Kirsch, L. Ruths, R. E. Brenner, J. Riegger, Senolytic therapy combining dasatinib and quercetin restores the chondrogenic phenotype of human osteoarthritic chondrocytes by the release of pro-anabolic mediators. *Aging Cell* **24**, e14361 (2025).
13. M. J. Yousefzadeh *et al.*, Fisetin is a senotherapeutic that extends health and lifespan. *EBioMedicine* **36**, 18–28 (2018).
14. X. Han *et al.*, Foxo4 peptide targets myofibroblast ameliorates bleomycin-induced pulmonary fibrosis in mice through ECM-receptor interaction pathway. *J. Cell. Mol. Med.* **26**, 3269–3280 (2022).
15. Y. Zhu *et al.*, The Achilles' heel of senescent cells: From transcriptome to senolytic drugs. *Aging Cell* **14**, 644–658 (2015).
16. L. J. Hickson *et al.*, Senolytics decrease senescent cells in humans: Preliminary report from a clinical trial of Dasatinib plus Quercetin in individuals with diabetic kidney disease. *EBioMedicine* **47**, 446–456 (2019).
17. A. R. Mendelsohn, J. W. Larrick, Cellular senescence as the key intermediate in tau-mediated neurodegeneration. *Rejuvenation Res.* **21**, 572–579 (2018).
18. A. Gadecka *et al.*, The senolytic cocktail, dasatinib and quercetin, impacts the chromatin structure of both young and senescent vascular smooth muscle cells. *Geroscience* **47**, 3907–3925 (2025).
19. G. Azizi, M. Goudarzvand, S. Afraei, R. Sedaghat, A. Mirshafiey, Therapeutic effects of dasatinib in mouse model of multiple sclerosis. *Immunopharmacol. Immunotoxicol.* **37**, 287–294 (2015).
20. A. Hochhaus, H. Kantarjian, The development of dasatinib as a treatment for chronic myeloid leukemia (CML): From initial studies to application in newly diagnosed patients. *J. Cancer Res. Clin. Oncol.* **139**, 1971–1984 (2013).
21. M. Breccia, G. Alimena, Activity and safety of dasatinib as second-line treatment or in newly diagnosed chronic phase chronic myeloid leukemia patients. *BioDrugs* **25**, 147–157 (2011).
22. H. L. Holen *et al.*, Signaling through ephrin-A ligand leads to activation of Src-family kinases, Akt phosphorylation, and inhibition of antigen receptor-induced apoptosis. *J. Leukoc. Biol.* **84**, 1183–1191 (2008).
23. M. Richardson, D. R. Richardson, Pharmacological targeting of senescence with senolytics as a new therapeutic strategy for neurodegeneration. *Mol. Pharmacol.* **105**, 64–74 (2024).
24. J. M. Al-Khayri *et al.*, Flavonoids as potential anti-inflammatory molecules: A review. *Molecules* **27**, 2901 (2022).
25. P. K. Deepika, Maurya, health benefits of quercetin in age-related diseases. *Molecules* **27**, 2498 (2022).
26. H. L. Hsieh *et al.*, Quercetin exerts anti-inflammatory effects via inhibiting tumor necrosis factor-alpha-induced matrix metalloproteinase-9 expression in normal human gastric epithelial cells. *World J. Gastroenterol.* **28**, 1139–1158 (2022).
27. E. Zoico *et al.*, Senolytic effects of quercetin in an in vitro model of pre-adipocytes and adipocytes induced senescence. *Sci. Rep.* **11**, 23237 (2021).
28. C. M. Roos *et al.*, Chronic senolytic treatment alleviates established vasomotor dysfunction in aged or atherosclerotic mice. *Aging Cell* **15**, 973–977 (2016).
29. A. K. Palmer *et al.*, Targeting senescent cells alleviates obesity-induced metabolic dysfunction. *Aging Cell* **18**, e12950 (2019).
30. A. Nambiar *et al.*, Senolytics dasatinib and quercetin in idiopathic pulmonary fibrosis: Results of a phase I, single-blind, single-center, randomized, placebo-controlled pilot trial on feasibility and tolerability. *EBioMedicine* **90**, 104481 (2023).
31. B. L. Torrance *et al.*, Senolytic treatment with dasatinib and quercetin does not improve overall influenza responses in aged mice. *Front. Aging* **4**, 1212750 (2023).
32. M. Xu *et al.*, Senolytics improve physical function and increase lifespan in old age. *Nat. Med.* **24**, 1246–1256 (2018).
33. C. C. Stolt *et al.*, SoxD proteins influence multiple stages of oligodendrocyte development and modulate SoxE protein function. *Dev. Cell* **11**, 697–709 (2006).
34. H. Huang *et al.*, Id2 and Id4 are not the major negative regulators of oligodendrocyte differentiation during early central nervous system development. *Glia* **70**, 590–601 (2022).
35. S. Wang, A. Sdrulla, J. E. Johnson, Y. Yokota, B. A. Barres, A role for the helix-loop-helix protein Id2 in the control of oligodendrocyte development. *Neuron* **29**, 603–614 (2001).
36. S. K. Ludwin, E. S. Johnson, Evidence for a "dying-back" gliopathy in demyelinating disease. *Ann. Neurol.* **9**, 301–305 (1981).
37. Q. L. Cui *et al.*, Sublethal oligodendrocyte injury: A reversible condition in multiple sclerosis? *Ann. Neurol.* **81**, 811–824 (2017).
38. M. S. Y. Yeung *et al.*, Dynamics of oligodendrocyte generation in multiple sclerosis. *Nature* **566**, 538–542 (2019).
39. T. Kuhlmann *et al.*, Differentiation block of oligodendroglial progenitor cells as a cause for remyelination failure in chronic multiple sclerosis. *Brain* **131**, 1749–1758 (2008).
40. Z. Liu *et al.*, Sec13 promotes oligodendrocyte differentiation and myelin repair through autocrine pleiotrophin signaling. *J. Clin. Invest.* **132**, e155096 (2022).

41. W. Lin *et al.*, Enhanced integrated stress response promotes myelinating oligodendrocyte survival in response to interferon-gamma. *Am. J. Pathol.* **173**, 1508–1517 (2008).
42. S. Wu, S. Stone, K. A. Nave, W. Lin, The integrated UPR and ERAD in oligodendrocytes maintain myelin thickness in adults by regulating myelin protein translation. *J. Neurosci.* **40**, 8214–8232 (2020).
43. M. Pennuto *et al.*, Ablation of the UPR-mediator CHOP restores motor function and reduces demyelination in Charcot-Marie-Tooth 1B mice. *Neuron* **57**, 393–405 (2008).
44. M. Kuroiwa *et al.*, Effect of amiloride on endoplasmic reticulum stress response in the injured spinal cord of rats. *Eur. J. Neurosci.* **40**, 3120–3127 (2014).
45. F. Pernin *et al.*, Diverse injury responses of human oligodendrocyte to mediators implicated in multiple sclerosis. *Brain* **145**, 4320–4333 (2022).
46. J. B. Grinspan, M. F. Reeves, M. J. Coulaloglou, D. Nathanson, D. Pleasure, Re-entry into the cell cycle is required for bFGF–induced oligodendroglial dedifferentiation and survival. *J. Neurosci. Res.* **46**, 456–464 (1996).
47. J. B. Grinspan, J. L. Stern, B. Franceschini, D. Pleasure, Trophic effects of basic fibroblast growth factor (bFGF) on differentiated oligodendroglia: A mechanism for regeneration of the oligodendroglial lineage. *J. Neurosci. Res.* **36**, 672–680 (1993).
48. F. Pernin *et al.*, Regulation of stress granule formation in human oligodendrocytes. *Nat. Commun.* **15**, 1524 (2024).
49. S. Stone, W. Lin, The unfolded protein response in multiple sclerosis. *Front. Neurosci.* **9**, 264 (2015).
50. A. N. Mhaille *et al.*, Increased expression of endoplasmic reticulum stress-related signaling pathway molecules in multiple sclerosis lesions. *J. Neuropathol. Exp. Neurol.* **67**, 200–211 (2008).
51. P. Cunnea *et al.*, Expression profiles of endoplasmic reticulum stress-related molecules in demyelinating lesions and multiple sclerosis. *Mult. Scler.* **17**, 808–818 (2011).
52. M. Absinta *et al.*, A lymphocyte–microglia–astrocyte axis in chronic active multiple sclerosis. *Nature* **597**, 709–714 (2021).
53. A. C. Geraghty *et al.*, Loss of adaptive myelination contributes to methotrexate chemotherapy-related cognitive impairment. *Neuron* **103**, 250–265.e58 (2019).